Estuarine, Coastal and Shelf Science 218 (2019) 119–130

Contents lists available at ScienceDirect

Estuarine, Coastal and Shelf Science

journal homepage: www.elsevier.com/locate/ecss

Characteristics of flow fluctuations in a tide-dominated estuary: Application of triple decomposition technique

Kabir Suara[a,*], Richard Brown[a], Hubert Chanson[b]

[a] Environmental Fluid Mechanics Group, Queensland University of Technology (QUT), QLD, 4000, Australia
[b] School of Civil Engineering, The University of Queensland, QLD, 4072, Australia

A B S T R A C T

Small tide dominated estuaries are affected by both large scale flow structures manifested as oscillatory residual currents and small scale bed generated turbulence. The present understanding of the effects and relative contributions of these factors are inadequate due to limited systematic observations. A field study was conducted in a small sub-tropical estuary in which high frequency (50 Hz) turbulence data were recorded continuously for about 48 h. A triple decomposition technique was introduced to isolate the contributions of tides, slow fluctuations and 'true' turbulence in the flow field. A striking feature of the data set was the slow fluctuations which exhibited large velocity amplitudes up to 50% of the tidal amplitude under neap tide conditions. The skewness of the fast 'true' turbulence were within the range of −4 and +2. The analysis of the fast fluctuations revealed that variation in the turbulence characteristics are linked with the tidal velocity suggesting that the dispersion and mixing are dependent on some large scale flow properties. The results also indicated enhanced mixing associated with the slow fluctuation in the flow field. The results provided useful sets of information about the properties of slow and fast fluctuating components and their variations through tidal cycles in a micro-tidal estuary.

1. Introduction

Mixing and dispersion in estuaries are complex phenomena due to the transition and strong competition between ocean and river processes. The circulation is driven by tidal flows, river discharge, energetic turbulence and rough bathymetry among other factors (Chen and Sanford, 2009; MacCready and Geyer, 2010). In an estuary, mixing has been identified to result from the combination of large scale advection and small scale turbulent diffusion (Fischer, 1976; Fischer et al., 1979). Turbulent mixing is generated by the frictional action of tidal inflow over the channel bed while large scale flow resulting in random eddy-like motion and organised seiche waves are often generated by the interaction of tide with bathymetry and structures in the vicinity of an estuary. Predictions of scalar transport and mixing caused by turbulence and large residual flow are often inferred and rarely accurate due to inadequate observations in small tidal estuaries.

The vast majority of estuaries in Australia are of the coastal type, particularly in the tropical and subtropical regions (Digby et al., 1999). They are characterized with features such as a funnel-like shape and meanders and are protected from direct action of waves by being discharged into semi-protected bays. These small estuaries have a small volume, low flow and short flushing times relative to that of adjoining bays and thus often experience pronounced tidal and seasonal fluctuations in water quality variables (Uncles et al., 2014a). The topography and the dynamics of bays that small estuaries discharge into play an important role in their flow properties. Eprapah Creek-a small subtropical estuary exhibiting a micro-tidal condition with peak streamwise velocity ~0.3 m/s - is an example of such tidal dominated estuary. It discharges into Moreton Bay which is behind islands (Moreton Island and North Stradbroke Island) and separated from the coast.

Previous high frequency observations in estuaries have shown that the flow field fluctuations can be broadly categorized into the tidal, slow and fast fluctuations (Trevethan et al., 2008a). Tidal fluctuations are oscillations in the flow field related to the tidal frequencies while the fast fluctuations (herein, also referred to as the 'true' turbulence) occupy higher frequencies and are generated by the frictional action of tidal inflow over the channel bed and stratified shear effects (Trevethan et al., 2008a). Herein, slow fluctuations are described as those occupying the frequency range between tidal and fast fluctuations. Slow fluctuations which are related to seiche wave reflection and long-period infragravity waves from landmarks and structures that are both internal and external to estuarine channel have been observed in small estuaries (Chanson et al., 2012; Uncles et al., 2014b). In addition, interaction of tidal inflow and other low frequency fluctuations with internal structures of estuarine channels (e.g. meanders, vegetation and banks) can generate large scale eddies, with length and time scales larger than those generated by friction against the bed and, existing at the same frequency band as seiche waves in small estuaries. Thus, the slow

* Corresponding author. Environmental Fluid Mechanics Group, Science and Engineering Faculty, Queensland University of Technology, 2 George St., Brisbane, QLD, 4000, Australia.
E-mail address: k.suara@qut.edu.au (K. Suara).

https://doi.org/10.1016/j.ecss.2018.12.006
Received 5 March 2018; Received in revised form 24 September 2018; Accepted 12 December 2018
Available online 14 December 2018

fluctuations in small estuaries likely contain both coherent and incoherent motions within the same frequency band. The presence of slow fluctuations in the flow and scalar fields have been observed in many small estuaries. For example (Breaker et al., 2007; Trevethan et al., 2007), reported flow frequency fluctuation with period ranging from 0.18 to 2.5 h which were linked with resonance while (Uncles et al., 2014b) observed fluctuation with period ~ 5 min linked with the infragravity waves in estuaries. Similarly, turbulent properties in small tidal estuaries have been significantly examined using high frequency data from acoustic Doppler velocimeters (ADV) for different tidal types (West and Oduyemi, 1989; Stacey and Ralston, 2005; Trevethan and Chanson, 2009). These studies have used the standard double decomposition approach separating the flow field into mean and fluctuating components. However, the relative contributions of the slow and fast fluctuations in velocities to mixing parameters are not well understood.

A standard means of separating the contributions of the instantaneous flow field is the *Reynolds decomposition* in which the mean and the fluctuating flow contributions are obtained through a form of time averaging/filtering (i.e. double decomposition – Equation (1)). For example an instantaneous streamwise, V_x is decomposed into:

$$V_x = \overline{V_x} + v_x \quad (1)$$

where $\overline{V_x}$ is the mean streamwise velocity component and v_x is the fluctuation of streamwise velocity around the mean. This technique is applicable to flows with a constant mean. A modification of the approach applicable to gradually varying flow is the use of $\overline{V_x}$ as a variable time average or running mean (low-pass filtered value) with step size less than the cut-off period T (Trevethan et al., 2007). The efficacy of the method depends on the selection of the period *T*, and the cycle-to-cycle consistency of the organised motions. While such decomposition provided detailed characteristics of the turbulent eddies via statistical analysis with the selection of appropriate cut-off period T, the method does not account for the existence of periodic slow fluctuations in the flow field. The decomposition of the flow field into more than two bands allows separate characterisation of the flow field components based on their periodicity and underlying physics (Gargett and Savidge, 2016).

A series of studies have been conducted in Eprapah Creek (Table S1). The results of these studies showed that the flow and scalar properties varied in time with periods comparable to tidal cycles (Chanson et al., 2012). The results showed that small estuaries exhibit turbulence parameters contrasting with those of larger estuaries and distinct behavior of turbulence properties in response to spring tidal forcing (Trevethan and Chanson, 2009). An important feature of the flow and scalar fields was the presence of long-term oscillations which were related to the interaction of the tide with internal structures of the channel (e.g. meanders, bends and banks) and external structures (e.g. nearby islands) (Chanson et al., 2012). The double decomposition technique used in these previous studies separated of flow fields into their mean and fluctuating components. The uniqueness of the present work includes the application of a triple decomposition technique that separates the instantaneous flow fields into those related to tide, slow fluctuation and fast fluctuation and the investigation of the characteristics of the slow and fast fluctuations in a small micro-tidal estuary.

In the triple decomposition (TD) technique, the instantaneous flow fields may be decomposed into a varying mean velocity component and the identified fluctuating fields. Flow field data collected at fixed location over a period of few tidal cycles would include tidal signal, slow fluctuations and fast fluctuations ('true' turbulence). Each occupies a different range in the energy spectrum. TD was applied to a laboratory flow, characterized by superimposed periodic waves coupled with turbulent motions (Hussain and Reynolds, 1972). The technique was previously applied to periodic turbulent flows and riverine flows with large coherent structure in open channels (Fox et al., 2005; Yossef and Vriend, 2011) and to describe turbulence in an urban flood (Brown and Chanson, 2012).

The aim of present work is to examine the characteristics of the slow and fast fluctuations in a small tidal estuary by applying a new triple decomposition technique that separates the flow field into its constituents. This paper presents the implementation of a triple decomposition analysis and characteristics of the resulting fluctuations. This paper is outlined as follows. This Section 1 presents the introduction and review of past related works. Section 2 describes the field conditions and the instrumentations. Section 3 describes the data analysis approach. Sections 4 and 5 present and discuss the results.

2. Materials and methods

2.1. Field description

The field study was conducted in the estuary of Eprapah Creek (Longitude 153.30° East, Latitude 27.567° South) - a subtropical creek located in eastern Australia (Table S1 - between September 29 and October 1, 2013. The estuarine zone extends to 3.8 km length with a typical semi-diurnal tidal pattern. The cross-sections were asymmetrical, deeper towards the right bank and widen toward the mouth. The estuary discharges into Moreton Bay, a semi protected bay separated from the coast by Moreton Island. Within the bay, there are other distinct islands (e.g. Peel Island), that can interact with flood tides entering into the branching channels. These geometrical features play an important role in the transport of materials in the branching channels. Furthermore, Eprapah Creek is meandering, nourished by saline water and bordered by mangrove trees, which protect the surface water and boundaries from direct wind and erosion. The average tidal range during the field study was 1.2 m, while the local water depth at the sampling location (site 2B) at high tide was between 2.5 m at high tide and 0.9 m at low tides. The sampling location was site 2B (Fig. 1), 2.1 km from the mouth. The bed composition at sampling location (site 2B) changed from muddy fine silt at the banks to relatively large gravels and rocks in the middle. This changed the bed roughness friction rapidly and could alter the properties within the turbulent boundary layer (Suara et al., 2015). The total rainfall for September 2013 was between 17 and 23 mm at the weather stations within 20 km radius of the catchment and the cumulative rainfall for the last 7 days immediately prior to the field study was nil (ABM, 2018). The river discharge was insignificant. Freshwater discharge from the Victoria sewage treatment plant 2.6 km from the mouth, i.e. upstream the sampling location could influence the measurements at site 2B. The wind speed was 1.5 m/s on average from the North-North-East direction during the duration of the field study (Suara et al., 2015).

2.2. Instrumentation and quality control

Instantaneous velocities were measured with three ADV Sontek™ microADVs. The ADV1 was a 3D side-looking probe micro-ADV (16 MHz), the ADV2 was a 2D side-looking probe micro-ADV (16 MHz) and the ADV3 was a 3D down-looking probe micro-ADV (16 MHz) (Table 1). The ADVs were mounted on a bracket held outside of structural poles such that the wakes did not affect the sampling volumes, as observed visually. The ADVs were sampled continuously at 50 Hz with the sampling volumes located vertically above each other, at 0.32 m, 0.42 m and 0.55 m above the bed (Fig. 1). Instantaneous water elevations were measured with the pressure sensor installed in the ADV1. Water quality parameters were obtained using two self-logging multi-parameter water quality probes (YSI 6600) deployed next to the bed and free surface. Both probes were sampled at 0.1 Hz and measured conductivity, salinity, temperature, pH, dissolved oxygen, chlorophyll A and turbidity. Manual samples of water quality parameters and water elevation were additionally obtained. Table 1 lists the instruments deployed during the field experiments.

The ADV data sets were post-processed by removal of communication errors, data with correlation less than 60% and signal-noise-ratio

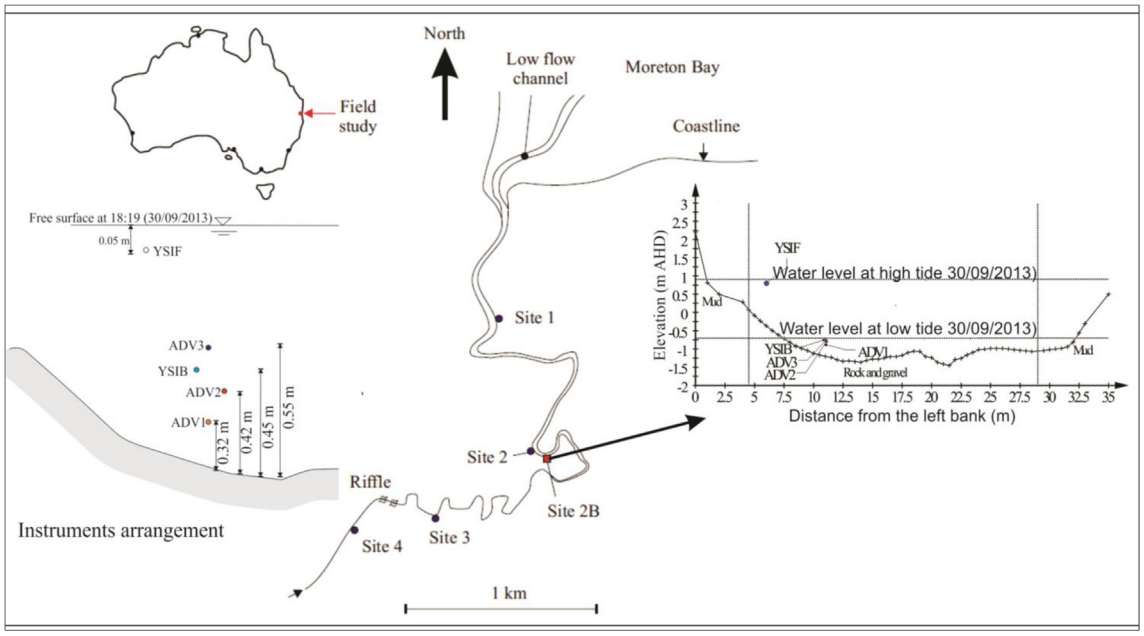

Fig. 1. Eprapah Creek estuarine zone (Longitude 153.30° East, Latitude 27.567° South), including surveyed sampling cross section on 29 Sept. 2013 and instrumentation arrangement.

less than 5 dB (Brown and Chanson, 2012). The data sets were also despiked using the phase-spaced thresholding technique (Goring and Nikora, 2002). Less than 5% of all the ADV data were removed after the processing. Spurious data points were replaced with last valid data point. The ADV times were synchronised to the nearest 0.02 s.

3. Data analysis approach

3.1. Triple decomposition of the flow field

As discussed in the introduction, the instantaneous velocity and water elevation time series in Eprapah Creek exhibit superposition of slow fluctuations with periods less than the tidal fluctuation. Therefore a triple decomposition can be applied (Brown and Chanson, 2013). Herein, instantaneous velocities and pressure were decomposed as:

$$V_i = \langle V_i \rangle + [V_i] + v_i \quad (2)$$

where $< V_i >$ is the tidal signal, $[V_i)$ is the slow fluctuation, v_i is the fast fluctuation and subscripts i represents x, y and z in the streamwise, transverse and vertical directions respectively. Fig. 2 shows a hypothetical power spectrum of an instantaneous field indicate the frequency range occupied by the velocity components in Eq. (2). Herein $< V_i >$ is the low-pass filtered data with a cut-off frequency of F_{cl}. The fast fluctuating component, v_i is the high-pass filtered data with the cut-off frequency F_{cu} while the slow fluctuating component $[V_i]$ is obtained by subtracting the sum $< V_i > + v_i$ from the instantaneous

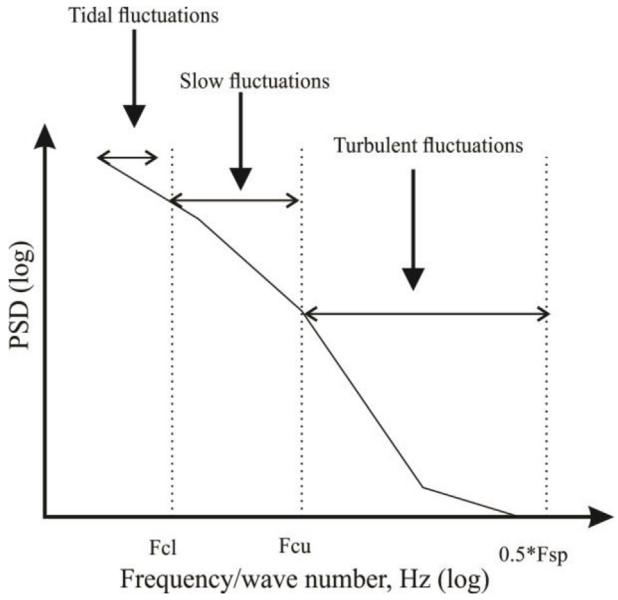

Fig. 2. Sketch of a hypothetical power spectral density of an instantaneous field flow measured in a tidal channel.

Table 1
Sampling and location information for instruments deployed at site 2B

Instrument code	Instrument description	Sample location	Sampling frequency
(1)	(2)	(3)	(4)
ADV1	Sontek 3D-sidelooking microADV A813F (16 MHz)	0.32 m above the bed 11.056 m from the left bank	50 Hz
ADV2	Sontek 2D-sidelooking microADV A641F (16 MHz)	0.42 m above the bed 11.042 m from the left bank	50 Hz
ADV3	Sontek 3D-downlooking microADV A843F (16 MHz)	0.55 m above the bed 11.05 m from the left bank	50 Hz
YSIB	YSI 6600 multi-parameter probe	0.45 m above the bed 10.866 m from the left bank	0.1 Hz
YSIF	YSI 6600 multi-parameter probe	0.05 m from the free surface	0.1 Hz
MW6	MW600 Dissolved oxygen meter	Manual sampling	Every 15 min
HI9	HI 98130 HANNA pH/Conductivity/TDS Tester	Manual sampling	Every 15 min

flow field occupying frequencies between F_{cl} and F_{cu}. Similarly to the double decomposition approach, triple decomposition defined using Eq. (2) implies that there is gap in the velocity spectrum for which many field observations have shown that such gap does not exist in environmental flows (LaCasce, 2008). Therefore, a key consideration was the determination of the characteristic frequencies (upper and lower cut-offs) that give most meaningful physical interpretation of the components.

Butterworth 2nd-order digital filter was employed in the low and high pass filtering. The filter was implemented with a "filtfilt" function in MATLAB that ensures zero phase shift and doubles the order of the filter which resulted in a 4th order filter herein (Gustafsson, 1996). The accuracy of filtering process was tested by reconstructing a velocity time series from its low and high-pass components at the selected frequencies. The RSME between the actual and reconstructed signals was $< 10^{-10}$ m/s, and had coherence of 1 with zero phase angle at all frequencies.

3.1.1. Characteristic frequencies

The decomposition of the instantaneous flow field was performed based upon characteristic frequencies (F_{cl} & F_{cu}). These were identified by visual observations, power spectra analyses and celerity of water within the channel. Although the flow field in the channel was unsteady, the goal was to choose cut-off frequencies that provided appropriate isolation of its constituents.

3.1.1.1. Selection of lower cut-off frequency F_{cl}. In the present study, in addition to the tidal oscillation, visual inspection of the velocity time series revealed some slow fluctuation; the largest with period of about 3000 s. Distinctive fluctuations were also observed in the power spectral plots of instantaneous data for velocity (Fig. 3b). Fig. 3 shows the spectra of velocity and water elevation with smoothed curves highlighting distinctive peaks and troughs in the power spectrum of the instantaneous data (ADV1) at frequencies greater than 0.00004 Hz. This fluctuation corresponds to a semi-diurnal tidal flow. The subsequent peaks and troughs suggested some energetic event with frequencies (around $F = 0.001$ Hz) corresponding to the visually observed slow fluctuations. Some sensitivity analyses were conducted on the flow field data to investigate the effects of the cut-off frequencies on the decomposed velocity components and pressure (Fig. 3). The results indicated that $< V_i >$ with cut-off frequency F_{cl} less than 0.0001 Hz is slightly affected by phase shift, while $< V_i >$ contained some signatures of the slow fluctuation for F_{cl} greater than 0.0001 Hz (see Fig. 4).

The major harmonic constituents of a semidiurnal tide are the principal lunar M2 and the luni-solar constituents K2. The spring-neap cycle and tidal range are determined by the difference in speeds and amplitudes of these components and other constituents. In addition, slowly varying mean due to subtidal and wind fluctuations have some influence on the tidal constituent causing cycle-cycle variation. These long period fluctuations were not captured in the 48 h dataset thus, difficult to obtain a precise frequency and amplitude for defining tidal constituents of the flow field. For longer period datasets, empirical mode decomposition (Huang et al., 1998) and multiple decimate and interpolate method (Gargett and Savidge, 2016) can be applied. The minor tide during the field experiment had a period of 42,660 s. Based on the sensitivity analysis of the lower cut-off frequency for the Eprapah Creek field data and other field data obtained in a similar semidiurnal channel, Mayes Canal at the Sunshine Coast, Australia (data not presented), the lower cut-off frequency using the triple decomposition technique described herein can be obtained using Equation (3):

$$\frac{4}{P_{\min}} \leq F_{cl} < \frac{1}{P_{fluc}} \tag{3}$$

where $F_{cl.}$ is the lower cut-off frequency which fulfil the Nyquist condition, $P_{\min}$ (herein ~42,000 s) is the period of the shortest tidal cycle observed and P_{fluc} (herein ~3000 s) is period of prominent slow fluctuation simultaneously observed in the water elevation and velocity measurements.

3.1.1.2. Selection of upper cut-off frequency, F_{cu}. The aim here was to select an upper cut-off frequency to isolate the fast fluctuation through a high-pass filter, by removing the large-scale fluctuations (tides and slow fluctuation). This was done by evaluating the effect of the upper cut-off frequency on the ensuring turbulence statistical properties which are expected to converge to some local values. The skewness, *Sk* (Equation (4)) is an essential diagnostic for determining F_{cu} because of its relationship with fluid eddy physics (Grass, 1971; Fox et al., 2005);

$$Sk(v_i) = \frac{\frac{1}{n}\sum_n v_i^3}{\left(\frac{1}{n}\sum_n v_i^2\right)^{3/2}}, \quad i = x, y, z \tag{4}$$

Other turbulent properties include, integral time scale, cross correlation coefficients, and standard deviation ratios (Suara et al., 2015). A complementary parameter that converged to a unique value

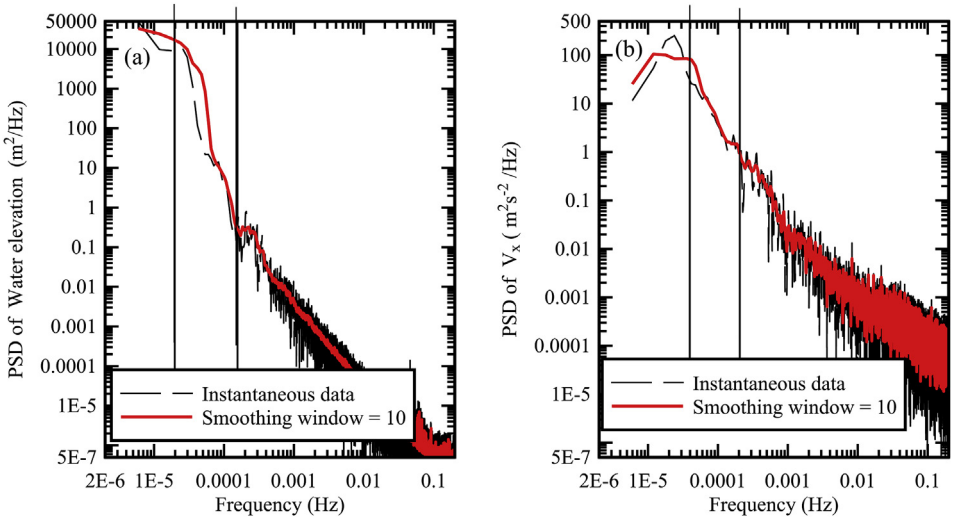

Fig. 3. Spectral analysis of fluctuations of (a) streamwise velocity V_x and; (b) water elevation measured using ADV1; Sampling volume location: 0.32 m above the bed, 11.06 m from left bank; Vertical lines indicate frequency range where F_{cl} could be located.

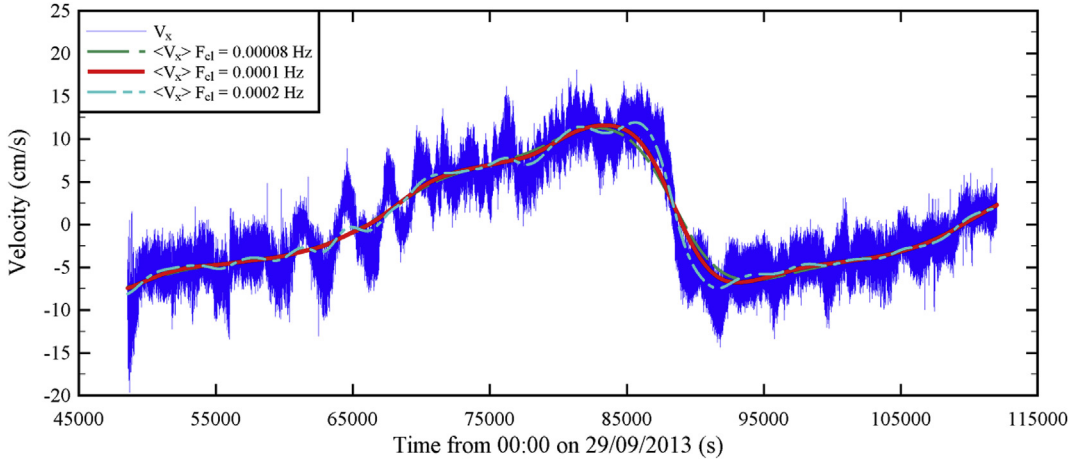

Fig. 4. Effect of the upper cut-off frequency on the approximation of the tidal component of velocity. ADV1 Sampling volume location: 0.32 m above the bed, 11.056 m from left bank.

independent of tidal phase was the integral time scale, T_E. T_E is obtained as the integral sum of a normalised autocorrelation function, R:

$$R_{ii}(\tau) = \frac{\overline{v_i(t)v_i(t+\tau)}}{\overline{v_i^2}}, \quad i = x, y, z \tag{5}$$

The skewness and integral time scale for the streamwise velocity of ADV1 data converged to unique value independent of tidal phase at frequencies $F \sim 0.2$ Hz (Fig. 5). For example, the skewness converged to a value around 0, expected of a Gaussian distribution at 0.2 Hz. The analyses with other ADV units and velocities components resulted in F ranging between 0.01 and 0.5 Hz. Other turbulence parameters showed no discernible relationship with the upper cut-off frequency (Suara et al., 2015).

Since the goal of F_{cu} selection is to ensure the fast fluctuation does not contain seiche wave motion, a more intuitive way to inform its selection is from the estimate sloshing period of shortest wave using Merian's equation:

$$T_{res} = 2l/\sqrt{gd} \tag{6}$$

where l is the distance between landmarks, g is the gravitational acceleration and d is the water depth. Table S2 summarises the properties of landmarks that are likely to contribute to seiche wave motion within Eprapah Creek using Equation (6). The first two rows describe seiches from external landmarks conceivably generated between the mouth of Eprapah Creek Channel and nearby islands within Moreton Bay while the others are linked with geometrical structures within the channel. The fastest seiche corresponded to that generated by the width of the channel at the sampling location which was approximately 25 m at low tide (30/10/2013) and corresponded to $T_{res.} \approx 16$ s (Equation (5)). Hence a characteristic frequency around 0.063 Hz was obtained. Thus, in addition to frequency range suggested by the ensuring turbulent statistics, an upper frequency of 0.1 Hz is applicable to separate the slow and fast fluctuations from the instantaneous flow fields.

From Eq. (2), the slow fluctuation (band-pass filtered data) was obtained by subtracting the sum of the tidal components (low-pass filtered data) and the fast fluctuation (high-pass filtered data) from the instantaneous flow fields. It is worth noting that the tidal components and the fast fluctuations were obtained from direct filtering of the instantaneous flow field. Therefore, the lower cut-off frequency had no effect on the resulting fast fluctuation and the upper cut-off frequency had no effect on the tidal components.

3.2. Turbulence analysis

In the followings, $F_{cl} = 0.00001$ Hz and $F_{cu} = 0.1$ Hz. Fast fluctuations are described in terms of standard deviations (and ratios), kinetic energies and integral time scale. Estimates of some turbulence statistical properties, correlations and Reynolds stresses are discussed with greater details in Suara et al. (2015).

Standard deviation is calculated based on finite number of discrete data as:

$$v_i' = \frac{1}{n}\sum_n \sqrt{(v_i - \overline{v_i})^2} = \frac{1}{n}\sum_n \sqrt{(v_i)^2}, \quad i = x, y, z \tag{7}$$

where over-bar signifies the mean which is zero, herein. The turbulence ratios (anisotropy) are obtained by normalising v_y' and v_z' with the

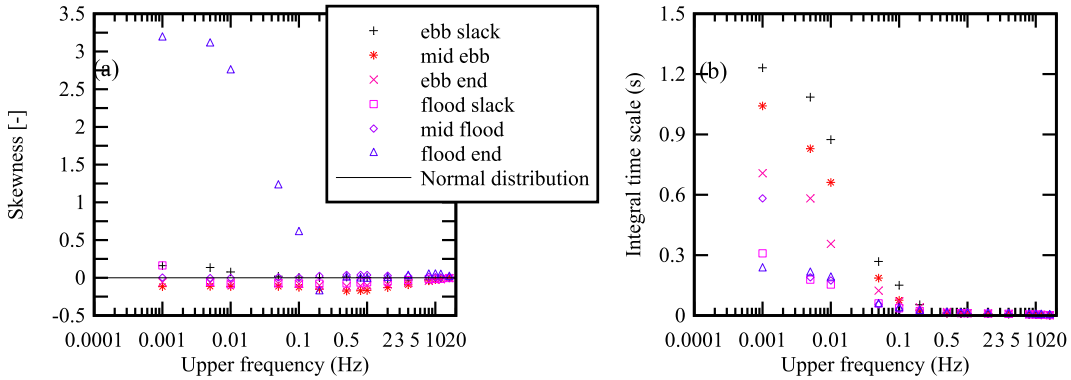

Fig. 5. Effect of cut-off frequency on (a) skewness and; (b) integral time scale of the streamwise turbulence velocity (high-pass filtered data) for data taken at some distinct tidal phases (See legend) ADV1; sampling volume location: 0.32 m above the bed, 11.06 m from left bank.

corresponding v_x' values.

The characteristic time scales were calculated from the autocorrelation function of the turbulent velocities. The normalised autocorrelation function, R describes the evolution of the turbulence field with time. R (Equation (5)) describes how a turbulence velocity correlates with values at difference time lag. The integral time scale is a measure of the correlation time between turbulent velocities. The integral length scale, e.g. T_{Ex} is the integral of the autocorrelation function which is obtained herein by numerical integration of R performed only up to the time of the first zero crossing using a maximum time lag of 10 s. Further increment in the lag value did not significantly alter the magnitudes of $T_{E.}$ Shear dominated turbulence has a length scale dependence on the distance from the bed. However, herein the integral scale is reported in time scale to avoid uncertainty with estimate of convective velocity due to unsteadiness of the mean flow and proximity to solid boundaries (Kim and Hussain, 1993; Bernard and Wallace, 2002).

4. Results and observations

4.1. Basic flow field and scalar observations

4.1.1. Instantaneous flow fields

Consistent with the previous field observation in Eprapah Creek (Table S1), the streamwise velocity, V_x is positive downstream (i.e. towards the mouth of the Creek, based on the channel centre at low tide), the transverse velocity, V_y is positive towards the left bank and the vertical velocity, V_z is positive upwards. Since the coordinate system is located on a bend in a tidal flow the streamwise direction varies resulting in a noticeable transverse, V_y, component at certain points in the tidal cycle. The instantaneous velocity and pressure data showed some substantial fluctuations in Eprapah Creek. The data contained the superimposition of pseudo-periodic fluctuations of different periods and amplitudes. Fig. 6 shows the instantaneous velocity and water elevation as functions of time for the field study. The streamwise velocity showed strong tidal incursion about low tide with the maximum velocities around 0.19 m/s and 0.16 m/s during the late ebb and early flood tides, respectively. Similar flood and ebb tide maxima were observed at various locations in Eprapah Creek (Trevethan et al., 2008a, 2008b; Chanson et al., 2012). The maximum velocity was on an average greater during the ebb than the flood tide. The transverse velocity data showed some tidal influence linked with the characteristics of the meander downstream of site 2B (Fig. 1).

4.1.2. Water quality parameters

The time series of the conductivity and pH measured simultaneously near the surface and next to the bed showed that the water quality parameters varied with tidal cycle (Fig. 7). The conductivity, pH and dissolved oxygen (Suara et al., 2015), which are solute properties varied with water elevation with peak values observed at high tides. The turbidity and chlorophyll A (not shown) varied with the tidal inflow velocity with peak values coinciding with periods of peak velocity around low tides. In general, the physio-chemistry of the channel suggested that the water column was reasonably mixed for temperature DO, turbidity and chlorophyll while it was partly stratified in terms of pH. Vertical gradient of conductivity and density were observed around high water while the low water exhibited well mixed condition. One possible cause of the vertical gradient of density and the pH was the fresh water discharge from the Victoria sewage treatment plant upstream the study location as no natural fresh water was observed during the field study.

The field experiment was not set-up to measure the local Richardson number, a measure of level of stratification within the channel. The approximate local Richardson number using density and velocity gradients at the locations of the instruments ranged from 1 to 100, indicating transition from well-mixed to fully stratified system (Trevethan and Chanson, 2009). This stratification and de-stratification of the channel is likely to influence the vertical momentum transport and some turbulent parameters within the channel (Trevethan and Chanson, 2009).

Similar to the flow velocity, the time variation of pH, dissolved oxygen and chlorophyll showed some marked oscillation with a period, $t \sim 3000$ s during the field experiment. These oscillations with an approximately 15 km wavelength occurred throughout the tidal study but were more pronounced during high-tide. The wavelength was obtained based on the first mode of natural resonance having a period $T_{res} > 3000$ s assuming an average depth of 10 m at high tide. This large wavelength was significantly larger than the 2.1 km, the distance of site 2B from the channel mouth (Table S2). Therefore, these fluctuations were possibly linked with reflection of tidal forcing from outside the channel (Trevethan et al., 2008b; Suara et al., 2015). Fluctuations with periods of about 6000 s and 10,000 s were observed with conductivity (Fig. 7) as well as chlorophyll and dissolved oxygen.

4.2. Properties of flow field components

The triple decomposition was applied to the raw instantaneous velocities using cut-off frequencies. Herein $< V >$ was the low-pass filtered data with a cut-off frequency of 0.0001 Hz (1/10,000 s^{-1}). The slow fluctuating component [V) was the band-passed data with the upper and lower cut-off frequencies set at 0.1 Hz and 0.0001 Hz (1/10 s^{-1} and 1/10,000 s^{-1} respectively). The turbulent component v was the

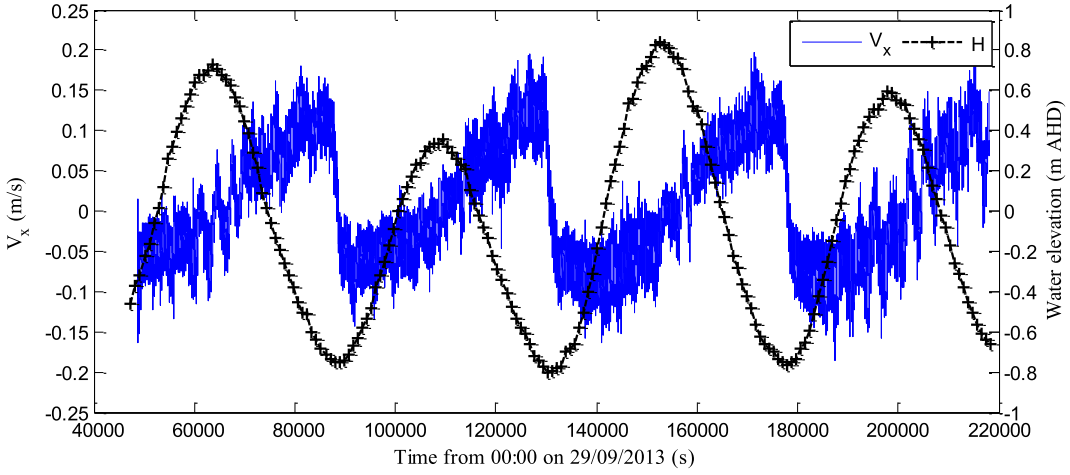

Fig. 6. Instantaneous longitudinal velocity V_x and water elevation as functions of time; data collected at 0.32 m above the bed and 11.06 m from the left bank.

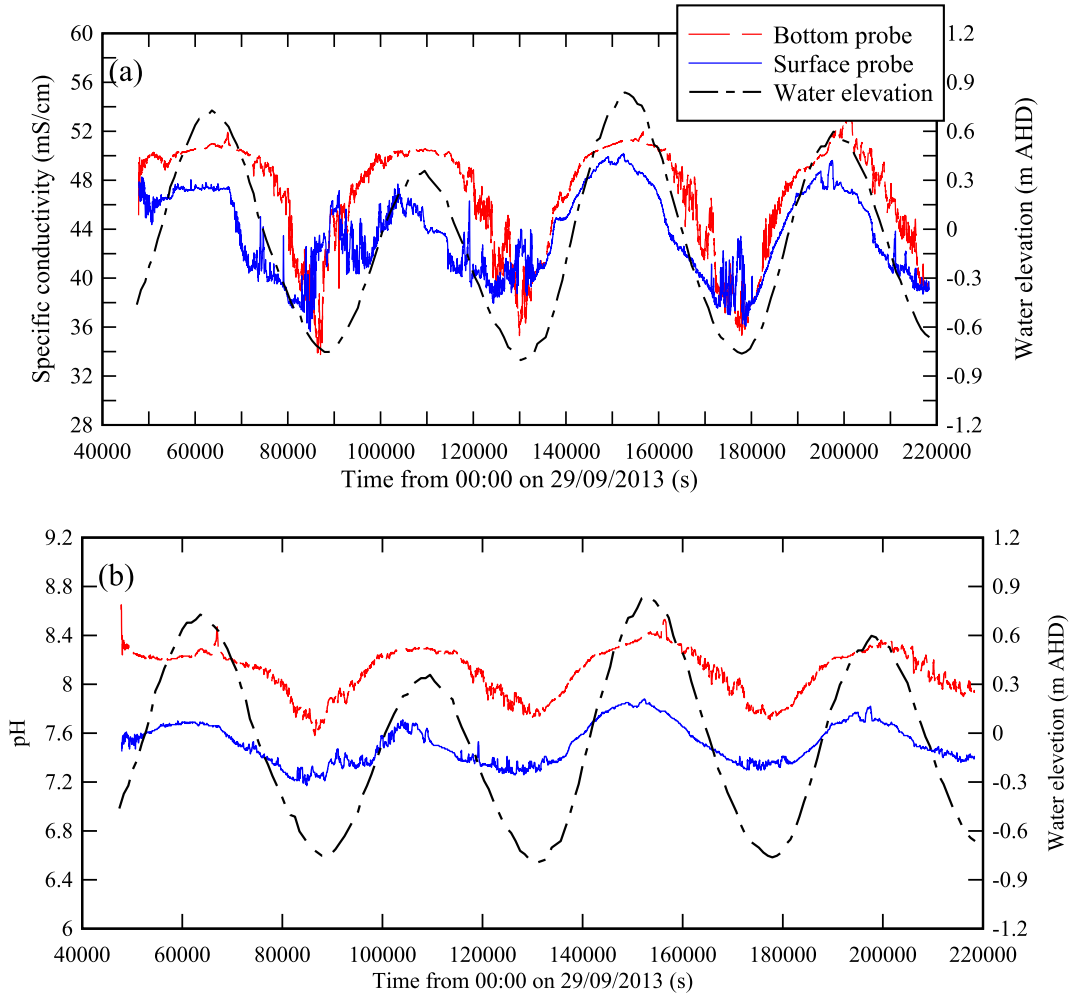

Fig. 7. Measured water conductivity, pH and water elevation as functions of time.

high-pass filtered data with a cut-off frequency of 0.1 Hz (1/10 s^{-1}). All statistical properties of the turbulent velocity components were calculated over a 200 s interval (10,000 data samples) as Trevethan et al. (2008b). Statistical properties were not calculated for sections with more than 10% removed and flagged data during post-processing.

4.2.1. Tidal scale properties

Fig. 8 shows the time variation of the tidal-scale velocity components $< V_x >$ for data collected at 0.32 m above the bed. Tidal velocity maxima around 0.1 m/s for both the ebb and flood tides occurred around low tide. Ebb tidal velocity maxima were larger than those of the flood tides. The transverse tidal velocity $< V_y >$ similar to the streamwise component exhibited peak velocities around low tide. The

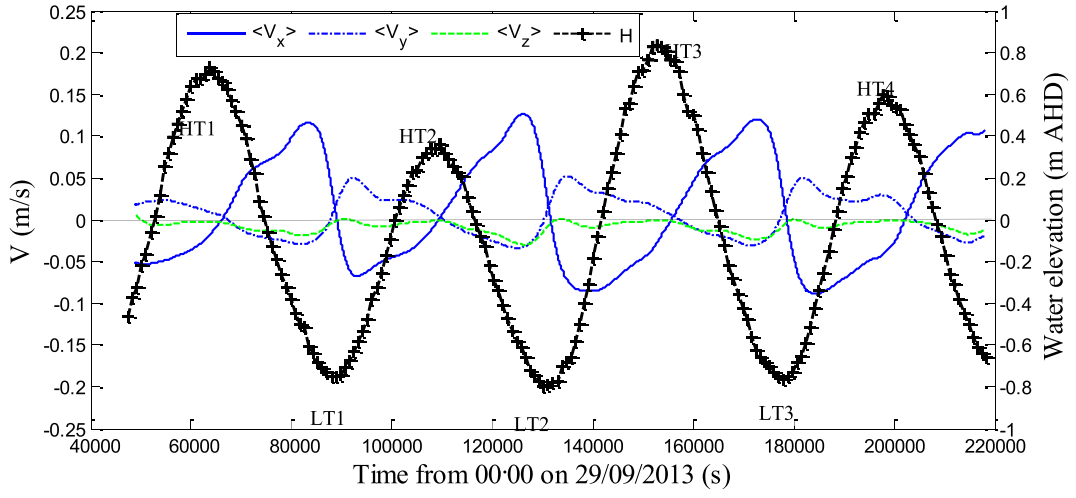

Fig. 8. Tidal components of velocity $< V_i >$ data collected at 0.32 m above the bed and 11.06 m from the left bank.

large amplitude of the transverse flow, ~0.025 m/s, was related to the change in the flow direction as a result of the bend. The flood tides forced the current across the channel toward the outer boundary while the ebb receded through the inner boundary (Fig. 1). The magnitude of the tidal vertical velocity $< V_z >$ was approximately zero during the flood tides. The non-zero negative vertical velocity values during the ebb tides were related to the slope in the cross section of the channel where the ADVs were deployed.

Tidal waves traveling through a natural channel could either be a standing wave, a progressive wave or a mixed-type wave. The flow velocity and tidal elevation are out of phase by 90° (i.e. π/2) for a standing wave while they are in phase for a progressive wave. The duration between the change in direction of tidal waves and a corresponding change in flow is defined as the phase lag (Savenije, 2006). Phase lag depends on a combination of factors which includes but is not limited to tidal dynamics, frictional response to tidal forcing and shape of the estuary (Savenije, 2006; MacVean and Stacey, 2011). As the tides interact with a basin, the degree of reflection of the tidal wave determines whether the tides are standing waves or progressive waves. The tidal components of the velocity and water elevation (i.e. stage) from the decomposed signal are used to examine wave type and phase lag in Eprapah Creek.

Stage-velocity analysis revealed that high tide and low tide slacks occurred after high and low tides respectively, suggesting that the channel a mixed-type tidal wave. However the lag, which is the difference between the time of high or low tide to slack water ($< V_x >$ = 0 m/s), varied with cycle. The lags were obtained by subtracting the time when $< V_x >$ is equal to zero from the time for preceding peak in water elevation. In general, the response of the flow direction to barotropic pressure gradient was slower during at high tide compared to low tide. The low tides (LT) occurred between 8 and 15 min before the low tide slacks (LWS) while the high tides (HT) occurred between 13 and 43 min before the high water slack. The lag on consecutive cycles showed some high to low alternating pattern, e.g. high tides HT1 and HT3, in major tidal cycle, i.e. exhibiting larger amplitude as shown in Fig. 8, occurred about 42 min before high water slack (HWS) while HT2 during a minor tidal cycle occurred 15 min before slack water (Table S3). This cycle to cycle variation is likely linked with the presence of slowly varying mean including diurnal tidal asymmetry. Further separation of the tidal components into semi-diurnal tidal signal and longer period mean can be achieved using harmonic analysis for long dataset (> 14.5 days) (Pawlowicz et al., 2002) or peak identification and interpolation method for short dataset (Gargett and Savidge, 2016). Because the focus of this current work is on the turbulent fluctuations, this additional decomposition of the tidal component was not covered.

The tidal variations in streamwise velocity showed remarkably strong ebb flow that was consistent with the instantaneous data. The normalised phase lag between the HW and HWS ranged between 0.035π – 0.116π (assuming π = 6 h 12 min) indicating a mixed type wave. Thus Eprapah Creek falls into the category of alluvial estuaries which are described with a typical phase lag 0.3 (π/10.42 radians) indicative of the ratio of bank convergence to tidal wavelength (Savenije, 2006).

4.2.2. Properties of slow fluctuations

Slow fluctuations were isolated into the band-pass component of the instantaneous flow field i.e. $[V_i]$ and exhibited oscillatory residual velocity after removing the tidal component. Fig. 9A shows the time variation of the slow fluctuation of the streamwise velocity for data collected at 0.32 m above the bed. The signal highlights some fluctuations which were most pronounced around slack tides and high waters (e.g. between 55,000 and 75,000 s; Fig. 9B). The slow fluctuations time series contained organised and repetitive seiches combined with random turbulent motion throughout the velocity data set. These seiches manifested as prominent peaks of energetic events while the turbulent motion manifested as a slope of −5/3 predicted by Kolmogorov's second similarity hypothesis within inertial sub-range in the velocity power spectral densities. In order to further confirm the existence of the seiches, coherence analysis between the different ADV units was carried out using the unfiltered velocity dataset. The result showed that there is coherence between velocities measured with the different ADV units for frequencies F < 0.05 Hz, at 95% confidence interval. Fig. 9B highlight two categories of slow fluctuations captured in the bandpass signal of the streamwise velocity and pressure data. The slow fluctuations with period $T > 3000$ s were often associated with interaction of the tide with external structure within Moreton Bay (e.g. Peel Island) while those with $T < 3000$ s were associated with structure such as meanders, width of the channel as estimated by the length of the resulting wave using Equation (5). The amplitude of the seiches were limited to ~0.02 m and ~0.002 m relative water elevation for those associated with external and internal structures, respectively and are shown with arrows in Fig. 9b. The corresponding velocity amplitudes in the streamwise direction were up to 0.08 m/s and 0.02 m/s for seiches associated with external and internal structures, respectively. Both categories showed a characteristic of a standing wave with the wave crests coinciding with the time of zero velocities as shown with the vertical reference lines at t = 60, 406 s and 63,764 s (Fig. 9 b).

4.2.3. Turbulence statistics

The fast fluctuation are analysed in terms of velocity standard deviations, integral time scales and their ratios in the spatial directions.

4.2.3.1. Standard deviations, and anisotropy. Standard deviation of turbulent velocity defines the magnitude of velocity fluctuations. Fig. 10a shows the standard deviation of instantaneous, slow and fast fluctuating, velocities as a function of time for the streamwise velocity recorded 0.32 m above the bed. The standard deviations followed a tidal trend with largest magnitude around low tides at periods of peak tidal velocity. The results showed that, on average, the standard deviation of the slow fluctuation was the same order of magnitude as that of the fast fluctuation. The standard deviations of slow fluctuation were higher during the flood tides than the ebb tides. Peak values were observed at the early part of flood tide owing to strong tidal forcing against topography coupled with interaction of the tides with inundated mangroves. The correlation of the standard deviation of velocities with the tidal inflow velocity is consistent with previous study in which eddy diffusivity obtained from Lagrangian drifters showed strong correlation with the tidal velocity (Suara et al., 2016). This suggested that the mixing and dispersion characteristics of the tidal channel are dependent on some large scale flow properties.

The degree of anisotropy in the flow was investigated to understand the directional structure of turbulence within the channel and its deviation from isotropic turbulence. In general the horizontal turbulence ratio $\acute{v}_y/\acute{v}_x$ mostly ranged between 0.3 and 0.9 (Table 2). These ratios agree well with laboratory observations in straight prismatic rectangular channel $\acute{v}_y/\acute{v}_x$ = 0.5–0.7 reported by Nezu and Nakagawa (1993) and smaller than values previously observed in Eprapah Creek during a spring tide $\acute{v}_y/\acute{v}_x$ ~1 (Trevethan et al., 2006). The magnitude of the turbulence ratio v_z'/v_x' at 0.32 m was close to isotropic and double that at 0.55 m above the bed. This suggested that the channel experienced rigorous vertical mixing due to bed friction, particularly at low tide during the neap tides. The horizontal turbulence ratio v_y'/v_x' showed some tidal trend, increased with an increase with streamwise velocity and had peaks around slack waters. The peaks around slack water were likely associated with lower streamwise velocity fluctuations. The horizontal turbulence ratios of the channel were on average higher during the flood tides than the ebb tides. Horizontal turbulence ratio increased from the bed.

The integral time scale of velocity, T_E is a measure of the longest connection between the fluctuating velocity components. Fig. 10b shows the time series of the integral time scale fast fluctuating

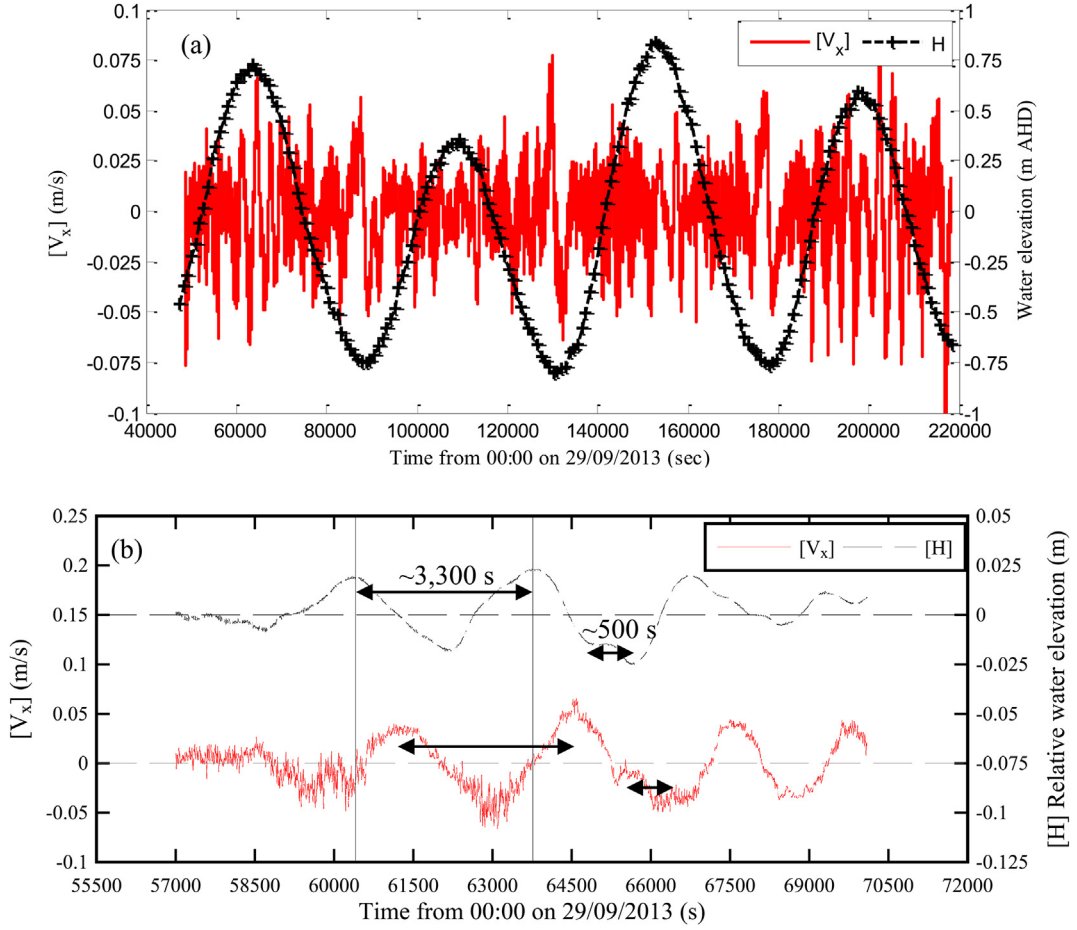

Fig. 9. Time series of slow fluctuating streamwise velocity [V_x) for ADV1 (a) for entire 48 h window; (b) for 4.2 h window highlighting the external and internal seiches: Arrow indicating wave periods with long and small corresponding to external and internal seiches, respectively; Sampling volume location: 0.32 m above the bed, 11.06 m from left bank.

velocities. All three components of T_E varied with increasing streamwise tidal velocity. On average, T_E was larger during the flood tide than during the ebb phase of the cycles. For all ADVs, the integral time scale for 'true' turbulence, T_{Ex} ranged from 0.01 to 0.5 s, while both T_{Ey} and T_{Ez} ranged from 0.01 to 0.7 s. The estimated integral time scale of the random signal in the slow fluctuation was two orders of magnitude higher than those presented in Table 2. The dimensionless integral time scales were on average T_{Ey}/T_{Ex} ~2.2 and T_{Ez}/T_{Ex} ~1. The average value was similar with that observed in mid-estuary where T_{Ey}/T_{Ex} ~1.7 (Trevethan et al., 2006). These ratios are higher than those observed in Eprapah Creek, Australia during a king tide T_{Ey}/T_{Ex} ~0.85 (Chanson et al., 2012) and in high energy tidal channel, Sound of Islay, UK T_{Ey}/T_{Ex} ~0.2 (Milne et al., 2013).

4.2.4. Additional turbulence properties

Reynold stresses, correlation, skewness and kurtosis of the ensued fast fluctuations were estimated and the key results are discussed herein. The three turbulent normal stresses had time averaged values for the floods and the ebbs ranging from 0.02 to 0.05 Pa while the time-averaged tangential Reynold stresses ranged between −0.02 and 0.02 Pa for all measured points. These results were slightly lower that the values observed during field study E6 (Table S1) with similar tidal height where the tangential stresses ranged between −0.08 and 0.08 Pa. This difference were likely associated with the scale of fluctuation isolated in the turbulence velocity. The normalised cross correlation R_{xz} showed strong relationship with the tidal velocity. The correlation coefficient R_{xz} diminished toward the bed similar to that of laboratory observation reported for turbulence in open channel flow (Kironoto and Graf, 1994). The skewness, *Sk*, estimated from Equation (3) and excess kurtosis, Ku, estimated from Equation (8), for all velocity components varied with streamwise velocity throughout the observation period ($Sk = 0$; $Ku = 0$ for Gaussian distribution).

$$Ku(v_x) = \frac{\frac{1}{n}\sum_n v_x^4}{\left(\frac{1}{n}\sum_n v_x^2\right)^2} - 3, \quad i = x, y, z \tag{8}$$

The skewness appeared within the range of −4 and +2. Over 65% of skewness values fell within the range expected of a finite Gaussian distribution - with N = 10,000 samples herein, $|Sk| < 4 \times (15/N)^{1/2}$ (Press et al., 1992) (Fig. S3). A quadrant analysis of the skewness distribution of the streamwise and vertical turbulent velocity with tidal phase was carried out (Fig. 11). The streamwise skewness values were predominantly negative during the ebb tides while the flood tides experienced mixed skewness. On the other hand, the skewness of the vertical turbulent velocity was mainly positive during the ebb. This suggested that the turbulence field close to bed contained eddies generated by ejection type processes during the ebb tides while the flood tides experienced both ejection and sweep type processes. However, the flood tides generated more eddies associated with high speed sweep against the bed (i.e. $v_x < 0$ & $v_z > 0$) than ejection type process (Nezu and Nakagawa, 1993; Buffin-Bélanger and Roy, 1998; Fox et al., 2005). The bulk of the excess kurtosis values (over 70%) fell within the range of −0.5 and + 2, slightly deviated from range expected of a finite normal distribution - with N = 10,000 samples herein, $|Ku| < 4 \times (96/N)^{1/2}$ (Press et al., 1992) (Fig. S3). Some event of very large kurtosis (magnitude up to 18) was observed and was possibly linked with

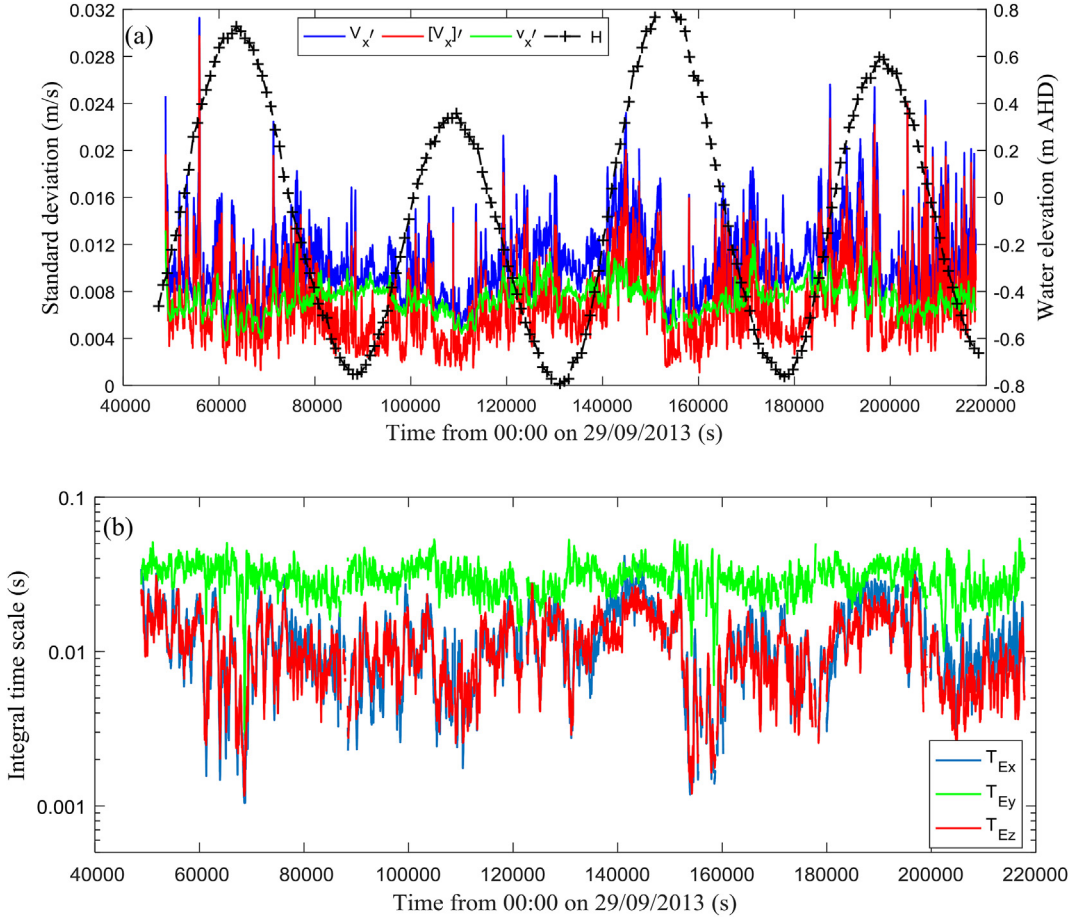

Fig. 10. Time variation of: (a) Standard deviation of the streamwise velocities (b) Integral time scale for data collected at 0.32 m above the bed, 11.06 m from left bank; Data based on 10,000 samples (200 s) every 10 s along the entire data set; V_x, $[V_x]$ and v_x are instantaneous, slow fluctuating and fast fluctuating velocities, respectively.

intermittency of the turbulence field and marine activities around the ADV probes (Fig. S4A). These turbulent properties are presented with greater details in (Suara et al., 2015).

5. Discussion

Water quality parameters and flow fields data were collected at high frequencies during a 48-h field study. The bulk physiochemical properties of the channel during the period of study indicated that the channel was reasonably well mixed and showed discernible tidal patterns. The conductivity and other measured solute properties varied with water elevation while the turbidity and chlorophyll *a* (particulate properties) varied with the streamwise velocity. The channel fluctuated between well mixed and fully stratified conditions. This stratification and de-stratification of the channel is likely to influence the vertical momentum transport and some turbulent parameters within the channel.

In order to examine the relative contributions of the slow and fast fluctuations in flow field to mixing parameters in the channel, a triple decomposition approach was applied. The technique allowed systematic separation of the contributions of the tidal, slow and fast fluctuations in the flow field based on their periodicity using digital filters. A vital benefit of the technique is to allow a characterisation of broader temporal scales of fluctuations of high frequency data sampled within a few tidal cycles. The decomposition approach can be extended to more than three categories depending on periodicity of physical

Table 2
Summary of characteristics (standard deviations and integral time scales) of fast fluctuations at three distances from the bed; Standard deviations are based on 10,000 samples (200 s) every 10 s along the entire data set; Data range (unshaded rows) is reported as 90% prediction bound around the average value (shaded rows).

ADV	z (m)	v_y'/v_x'	v_z'/v_x'	T_{Ex} (s)	T_{Ey} (s)	T_{Ez} (s)
1	0.32	0.3 – 0.8	0.9 – 1.1	0.01 - 0.42	0.03 - 0.54	0.01 - 0.31
		0.56	0.99	0.12	0.30	0.11
2	0.42	0.4 – 1.0		0.01 - 0.49	0.07 - 0.69	--
		0.73		0.16	0.28	
3	0.55	0.8 – 1.2	0.2 – 1.0	0.01 - 0.37	0.01 - 0.37	0.05 - 0.66
		0.96	0.59	0.13	0.12	0.25

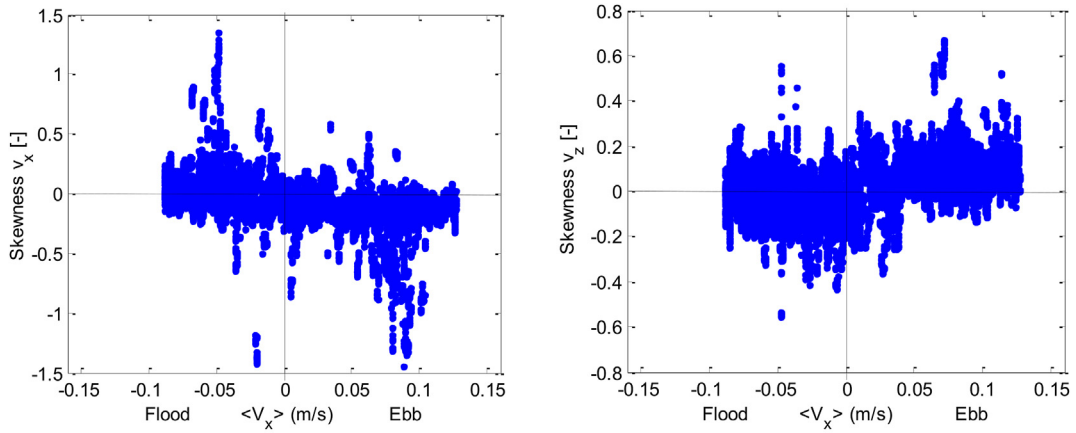

(A) Streamwise velocity skewness (B) Vertical velocity skewness

Fig. 11. Skewness distribution with tidal phase; Sampling volume location: 0.32 m above the bed, 11.056 m from left bank.

processes of interest. The tidal components contained combination of semi-diurnal flow fluctuations and slowly varying mean flow which was unresolved due to the short period of the observation. One important feature exhibited by the flow and scalar field observed within the channel was the presence of slow fluctuations. Analysis of the slow fluctuations showed the presence of seiches waves manifested as slow fluctuations in the time series of water elevation and velocity. The seiches were conceivably related to physical structures within and outside the channel. Although the amplitudes of the seiche waves were small relative to the tidal amplitude ($< 10\%$), they generated velocity amplitudes up to 50% of the tidal velocity component. The large amplitude fluctuations with period greater than 3000 s were associated with interaction of the tide with external forcing within Moreton Bay. On the other hand, slow fluctuations with periods less than 3000 s are features of tide interaction with topography, meanders and structures within the channel. The correlation between the slow fluctuations periods of the flow fields and the water quality parameters suggest their influence on transport and mixing within the channel.

So how could the oscillatory slow fluctuation affect the transport and mixing within the channel? Zimmerman (1986) discussed two possible mechanisms by which oscillatory currents and tides affect dispersion in tide dominated seas. The mechanisms are the “cascade” of shear dispersion and Lagrangian chaos. The “cascade” of shear dispersion involves transfer of energy through non-linear interaction of the bed generated turbulence with the vertical shear which in turn interacts with the horizontal shear created by the slow fluctuations. The latter mechanism relies on the randomisation of the flow field created by the superposition of arrays of organised motions in the Eulerian field which results in horizontal length scales larger than turbulence integral length scale. While it is difficult to identify which of these mechanisms dominated in Eprapah Creek during the period of the study, both mechanisms suggest that the slow fluctuations in the channel would result in a horizontal dispersion coefficient, which combines shear and smaller scale processes, significantly greater than bed generated eddy diffusivity. Using typical values of the velocity standard deviation and integral time scale for the fast fluctuation (Table 2), the bed generated eddy diffusivity was $\sim 10^{-4}\,m^2/s$. The standard deviation of the slow fluctuations was similar in magnitude with that of the turbulence while the integral time scale of the slow fluctuations was about two orders of magnitude greater. This scale argument suggests that the slow fluctuation would result in a horizontal shear dispersion coefficient at least two orders of magnitude higher than the turbulence eddy diffusivity within the channel. This scale analysis result is consistent with observation of diffusivity $> 0.01\,m^2/s$ using high resolution drifters in the same channel (Suara et al., 2016; Suara et al., 2017).

6. Conclusions

In this work, we examine the turbulence characteristics of the slow and fast fluctuations by applying a new triple decomposition technique which separates the tide, slow fluctuations and fast fluctuations in the flow field of a small tidal channel. A key benefit of the technique is to allow a characterisation of broader temporal scales of fluctuations of high frequency data sampled within a few tidal cycles. The analysis of the 'true' turbulence field showed some anisotropy similar to classical boundary layer results. The result showed that variation in the turbulence characteristics are linked with the tidal inflow. This suggested that the mixing and dispersion characteristics of the tidal channel are dependent on some large scale flow properties. Over 65% of skewness values fell within the range expected of a finite Gaussian distribution and ranged from -4 to $+2$. Additionally, analysis of the ‘true’ turbulence indicated that the ebb phase turbulence field was predominated by eddies that evolved from ejection type process while that of the flood phase contained mixed eddies with a significant amount related to sweep type process.

A key result of the investigation is characterisation of the slow fluctuations which combined seiches waves from landmarks inside and outside the estuary with random large scale turbulence motion. The standard deviations of the slow fluctuation were particularly large at high tides and were observed in the form of flow reversals around tide slacks. The average value of standard deviation of slow fluctuation was generally in the same range as that of the fast fluctuation (‘true’ turbulence). The estimated integral time scale of the incoherent signal in the slow fluctuation was two orders of magnitude higher than that of the true turbulence resulting in an estimate of diffusion coefficient at least two orders of magnitude higher than those related to the bed generated turbulence. In addition, the amplitudes of the seiche waves were small relative to the tidal amplitude ($< 10\%$) but significant as they generated velocity amplitudes up to 50% of the tidal velocity component. These indicate a significant contribution of the slow fluctuations to transport and mixing of scalar within the estuarine channel. The contribution of the slow fluctuations to transport and mixing is explained through the “cascade” of shear dispersion and the Lagrangian chaos mechanisms. Both mechanisms pointed to enhanced mixing resulting in larger horizontal dispersion coefficients.

Acknowledgments

The authors acknowledge the support from Dr Adrian McCallum in providing additional bathymetric data. They acknowledge the support received the following staff of University of Queensland (UQ), Australia; University of the Sunshine Coast (USC), Australia;

Queensland University of Technology (QUT), Australia in planning, implementing and providing logistics for the field study; Dr Badin Gibbes (UQ), Dr Alistair Grinham (UQ), Dr Hang Wang (UQ), Dr Helen Fairweather (USC), Dr Charles Wang (QUT), Dave McIntosh (QUT). They also acknowledge the support from the 2013 final year project students, James Kelly and Alex Wimsett in planning and carrying out the field work. The financial support of the Australian Research Council through linkage grants LP110100431 and LP150101172 is acknowledged.

Appendix A. Supplementary data

Supplementary data to this article can be found online at https://doi.org/10.1016/j.ecss.2018.12.006.

References

ABM, 2018. Australian bureau of meteorology. Available from: http://www.bom.gov.au/climate/data/index.shtml?bookmark=200, Accessed date: 25 April 2018.

Bernard, P.S., Wallace, J.M., 2002. Turbulent Flow: Analysis, Measurement, and Prediction. John Wiley & Sons.

Breaker, L.C., Broenkow, W.W., Watson, W.E., Jo, Y.-H., 2007. Tidal and nontidal oscillations in Elkhorn Slough, CA. Estuar. Coast 31 (2), 239. https://doi.org/10.1007/s12237-007-9021-8.

Brown, R.J., Chanson, H., 2012. Suspended sediment properties and suspended sediment flux estimates in an inundated urban environment during a major flood event. Water Resour. Res. 48 (11). https://doi.org/10.1029/2012WR012381.

Brown, R.J., Chanson, H., 2013. Turbulence and suspended sediment measurements in an urban environment during the Brisbane River flood of january 2011. J. Hydraul. Eng. 139 (2), 244–253. https://doi.org/10.1061/(asce)hy.1943-7900.0000666.

Buffin-Bélanger, T., Roy, A.G., 1998. Effects of a pebble cluster on the turbulent structure of a depth-limited flow in a gravel-bed river. Geomorphology 25 (3), 249–267.

Chanson, H., Brown, R.J., Trevethan, M., 2012. Turbulence measurements in a small subtropical estuary under king tide conditions. Environ. Fluid Mech. 12 (3), 265–289. https://doi.org/10.1007/s10652-011-9234-z.

Chen, S.N., Sanford, L.P., 2009. Axial wind effects on stratification and longitudinal salt transport in an idealized, partially mixed estuary. J. Phys. Oceanogr. 39 (8), 1905–1920. https://doi.org/10.1175/2009JPO4016.1.

Digby, M., Saenger, P., Whelan, M.B., McConchie, D., Eyre, B., Holmes, N., Bucher, D., 1999. A Physical Classification of Australian Estuaries. Land and Water Resources Research and Development Corporation, Canberra, Australia.

Fischer, H.B., 1976. Mixing and dispersion in estuaries. Annu. Rev. Fluid Mech. 8 (1), 107–133. https://doi.org/10.1146/annurev.fl.08.010176.000543.

Fischer, H.B., List, E.J., Koh, R.C., Imberger, J., Brooks, N.H., 1979. Mixing in Inland and Coastal Waters. Academic Press, New York.

Fox, J.F., Papanicolaou, A.N., Kjos, L., 2005. Eddy taxonomy methodology around a submerged barb obstacle within a fixed rough bed. J. Eng. Mech. 131 (10), 1082–1101. https://doi.org/10.1061/(ASCE)0733-9399(2005)131:10(1082).

Gargett, A.E., Savidge, D.K., 2016. Separation of short time series of currents into “fluctuations,” “tides,” and “mean” flow. J. Atmos. Ocean. Technol. 33 (5), 1089–1095. https://doi.org/10.1175/jtech-d-15-0232.1.

Goring, D.G., Nikora, V.I., 2002. Despiking acoustic Doppler velocimeter data. J. Hydraul. Eng. 128 (1), 117–126. https://doi.org/10.1061/(ASCE)0733-9429(2002)128:1(117).

Grass, A.J., 1971. Structural features of turbulent flow over smooth and rough boundaries. J. Fluid Mech. 50 (02), 233–255. https://doi.org/10.1017/S0022112071002556.

Gustafsson, F., 1996. Determining the initial states in forward-backward filtering. IEEE Trans. Signal Process. 44 (4), 988–992. https://doi.org/10.1109/78.492552.

Huang, N.E., Shen, Z., Long, S.R., Wu, M.C., Shih, H.H., Zheng, Q., Yen, N.-C., Tung, C.C., Liu, H.H., 1998. The empirical mode decomposition and the Hilbert spectrum for nonlinear and non-stationary time series analysis. In: Proceedings of the Royal Society of London A: Mathematical, Physical and Engineering Sciences, vol. 454. The Royal Society, pp. 903–995.

Hussain, A.K., Reynolds, W.C., 1972. The mechanics of an organized wave in turbulent shear flow. Part 2. Experimental results. J. Fluid Mech. 54 (02), 241–261. https://doi.org/10.1017/S0022112072000667.

Kim, J., Hussain, F., 1993. Propagation velocity of perturbations in turbulent channel flow. Phys. Fluid. Fluid Dynam. 5 (3), 695–706. https://doi.org/10.1063/1.858653.

Kironoto, B.A., Graf, W.H., 1994. Turbulence characteristics in rough uniform open-channel flow. Proc. ICE - Water Marit. Energy 106 (4), 333–344.

LaCasce, J., 2008. Lagrangian statistics from oceanic and atmospheric observations. Transport and Mixing in Geophysical Flows. Springer, pp. 165–218.

MacCready, P., Geyer, W.R., 2010. Advances in estuarine physics. Annual Review of Marine Science 2, 35–58. https://doi.org/10.1146/annurev-marine-120308-08101.

MacVean, L.J., Stacey, M.T., 2011. Estuarine dispersion from tidal trapping: a new analytical framework. Estuar. Coast 34 (1), 45–59. https://doi.org/10.1007/s12237-010-9298-x.

Milne, I.A., Sharma, R.N., Flay, R.G.J., Bickerton, S., 2013. Characteristics of the turbulence in the flow at a tidal stream power site. Phil. Trans. Math. Phys. Eng. Sci. 371 (1985). https://doi.org/10.1098/rsta.2012.0196.

Nezu, I., Nakagawa, H., 1993. Turbulence in Open-channel Flows. IAHR Monograph, IAHR Fluid Mechanics Section, Balkema, Rotterdam, The Netherlands.

Pawlowicz, R., Beardsley, B., Lentz, S., 2002. Classical tidal harmonic analysis including error estimates in MATLAB using T_TIDE. Comput. Geosci. 28 (8), 929–937. https://doi.org/10.1016/S0098-3004(02)00013-4.

Press, W.H., Teukolsky, S.A., Vetterling, W.T., Flannery, B.P., 1992. Numerical Recipes in Fortran 77: the Art of Scientific Computing. Cambridge University, Cambridge, England.

Savenije, H.H., 2006. Salinity and Tides in Alluvial Estuaries, first ed. ed. Elsevier BV, Amsterdam, The Netherlands.

Stacey, M.T., Ralston, D.K., 2005. The scaling and structure of the estuarine bottom boundary layer. J. Phys. Oceanogr. 35 (1), 55–71. https://doi.org/10.1175/JPO-2672.1.

Suara, K., Chanson, H., Borgas, M., Brown, R.J., 2017. Relative dispersion of clustered drifters in a small micro-tidal estuary. Estuarine, Coastal and Shelf Science 194, 1–15. https://doi.org/10.1016/j.ecss.2017.05.001.

Suara, K.A., Brown, R.J., Borgas, M., 2016. Eddy diffusivity: a single dispersion analysis of high resolution drifters in a tidal shallow estuary. Environ. Fluid Mech. 16 (5), 923–943. https://doi.org/10.1007/s10652-016-9458-z.

Suara, K.A., Brown, R.J., Chanson, H., 2015. Turbulence and mixing in the environment: multi-device study in a sub-tropical estuary. In: Report No. CH99/15, Div.of Civil Engineering. The University of Queensland, Brisbane, Australia1742721389, .

Trevethan, M., Chanson, H., 2009. Turbulent mixing in a small estuary: detailed measurements. Estuarine, Coastal and Shelf Science 81 (2), 191–200. https://doi.org/10.1016/j.ecss.2008.10.020.

Trevethan, M., Chanson, H., Brown, R.J., 2006. Two Series of Detailed Turbulence Measurements in a Small Subtropical Estuarine System. Report No. CH58/06. Div.of Civil Engineering, The University of Queensland, Brisbane, Australia1864998520.

Trevethan, M., Chanson, H., Brown, R.J., 2008a. Turbulence characteristics of a small subtropical estuary during and after some moderate rainfall. Estuarine, Coastal and Shelf Science 79 (4), 661–670. https://doi.org/10.1016/j.ecss.2008.06.006.

Trevethan, M., Chanson, H., Brown, R.J., 2008b. Turbulent measurements in a small subtropical estuary with semidiurnal tides. J. Hydraul. Eng. 134 (11), 1665–1670. https://doi.org/10.1061/(ASCE)0733-9429(2008)134%3A11(1665).

Trevethan, M., Chanson, H., Takeuchi, M., 2007. Continuous high-frequency turbulence and suspended sediment concentration measurements in an upper estuary. Estuarine, Coastal and Shelf Science 73 (1), 341–350. https://doi.org/10.1016/j.ecss.2007.01.014.

Uncles, R.J., Stephens, J.A., Harris, C., 2014a. Freshwater, tidal and wave influences on a small estuary. Estuarine, Coastal and Shelf Science 150, 252–261. https://doi.org/10.1016/j.ecss.2014.05.035.

Uncles, R.J., Stephens, J.A., Harris, C., 2014b. Infragravity currents in a small ría: estuary-amplified coastal edge waves? Estuarine, Coastal and Shelf Science 150, 242–251. https://doi.org/10.1016/j.ecss.2014.04.019.

West, J., Oduyemi, K., 1989. Turbulence measurements of suspended solids concentration in estuaries. J. Hydraul. Eng. 115 (4), 457–474. https://doi.org/10.1061/(ASCE)0733-9429(1989)115:4(457).

Yossef, M.F.M., Vriend, H. J. d., 2011. Flow details near river Groynes: Experimental investigation. J. Hydraul. Eng. 137 (5), 504–516. https://doi.org/10.1061/(ASCE)HY.1943-7900.0000326.

Zimmerman, J., 1986. The tidal whirlpool: a review of horizontal dispersion by tidal and residual currents. Neth. J. Sea Res. 20 (2), 133–154. https://doi.org/10.1016/0077-7579(86)90037-2.